ADVANCED INTELLIGENT SYSTEMS
Open Access
www.advintellsyst.com

# A Study on the Effect of Belly-Dragging Locomotion on a Robot that Mimics a Heavy Reptile

*Seunghyun Lim, Jinhyeok Song, and Dongwon Yun**

**This study investigates the effect of tortoise-inspired locomotion on enhancing energy efficiency in legged robots. Tortoises, known for their high locomotion efficiency, provide a unique model for robot and gait design, where their specific gait and posture significantly contribute to energy efficiency. This study hypothesizes that the gait and belly-dragging posture of tortoises can improve the energy efficiency of robots. To test this hypothesis, a quadruped robot mimicking these tortoise characteristics is developed, utilizing the cost of transport (CoT) as a measure of energy efficiency. Dynamic simulations and real-world experiments are conducted, varying parameters like robot size, mass, friction coefficient, and Froude number, to validate the generality of the findings. The results indicate that both belly dragging, a postural characteristic of tortoises, and their diagonal gait significantly lower the robot's CoT. This suggests that the energy-efficient locomotion of tortoises, specifically the diagonal gait with belly dragging, is transferable to robotic platforms to enhance energy efficiency. The tortoise-inspired robot design offers significant potential in applications such as search and rescue operations, space exploration, and payload transportation. Furthermore, the tortoise-inspired locomotion strategy can be effectively integrated with other research focusing on energy efficiency improvements through mechanical structures or control strategies.**

## 1. Introduction

Animals have various body structures and gaits with their characteristics. Recently, research applying various gaits of animals to legged robots has received significant attention.[1,2] Legged robots can be used for various purposes, such as delivery, guidance, driving, and searching of rough terrain because they can drive over irregular environments that wheel robots cannot overcome.[3–5] For this reason, studies are being conducted to imitate the characteristics of certain animals and apply them to legged robots; among them, several studies on quadruped robots and their gaits have been conducted.[6–11] A research group trained a quadruped robot by imitating the flexible movement of dogs to implement natural and stable movement.[12] In addition, an amphibious robot was proposed that mimics the characteristics of a turtle, which can move on both water and land.[13,14] An adaptive morphogenesis approach was used to facilitate the multienvironment transition of an amphibious legged robot by mimicking the limb shape and locomotion of turtle species.[15] As shown in these studies, biomimetic technology can implement certain functions or solve problems of legged robots for particular purposes.

Although legged robots have the advantage of being able to overcome various environments, they have disadvantages of lower load capacity and high energy consumption compared to wheel robots, and several studies have been conducted to overcome these problems.[16,17] There are several ways to improve the energy efficiency of robots, including the use of compliant actuators, dynamical analysis of segmented limbs, energy-efficient control methods, and locomotion principles.[18] Of these, research on locomotion principles utilizing bioinspired insight is based on observations and comparisons with animal biomechanics. For example, a study was conducted to enhance the load capacity of a cockroach-like robot, which was made of a smart composite microstructure, utilizing belly dragging, a motion inspired by the belly contact locomotion of lizards or crocodiles.[19] ATRIAS at Oregon State University utilized a spring-mass model inspired by the gait of an ostrich in their bipedal robot to achieve a high regeneration efficiency of 30%–40%.[20] Meanwhile, BirdBot at the Max Planck Institute for Intelligent Systems was developed with a multijoint elastic coupling mechanism that simulates the movement of emu cadaver leg joints, resulting in increased energy efficiency.[21] However, no prior research has been conducted to investigate the potential increase in energy efficiency that could be achieved by imitating the unique locomotion characteristics and advantages of tortoises. Against this backdrop of legged robotics and biomimicry, our study posits a novel hypothesis: by emulating the gait and belly-dragging posture of tortoises, we can significantly enhance the energy efficiency of robotic designs.

S. Lim, J. Song, D. Yun
Department of Robotics and Mechatronics Engineering
Daegu Gyeongbuk Institute of Science and Technology (DGIST)
Daegu 42988, Republic of Korea
E-mail: mech@dgist.ac.kr

The ORCID identification number(s) for the author(s) of this article can be found under https://doi.org/10.1002/aisy.202300720.



**DOI: 10.1002/aisy.202300720**

For numerically representing the energy efficiency of locomotion in various species or robots, the concept of a cost of transport (CoT) serves as a pivotal tool. CoT is a dimensionless quantity of locomotion efficiency in walking animals and robots, also referred to as specific resistance.[22] For instance, the CoT of a cockroach and an ostrich are 16.0 and 1.3, respectively, while their robotic counterparts, HARM-F at Harvard University and BirdBot at the Max Planck Institute for Intelligent Systems, have CoTs of 83.9 and 1.68, respectively.[21,23,24]

Tortoises are known for their high locomotive efficiency.[25] Generally, arthropods and vertebrates satisfy an allometric relationship with a minimum CoT $C_m = 10.8\,M^{-0.31}$, where $M$ is their mass.[26] However, the terrestrial locomotion of short-necked turtles shows a CoT of 5.97, which is less than half of the predicted minimum CoT (12.55).[27] Similarly, Mediterranean spur-thighed tortoises have a minimum CoT of 4.11, which is lower than the predicted value (14.78).[28] Based on these research findings, it can be understood that tortoises perform efficient terrestrial locomotion relative to their mass.

One reason for these results is that tortoises have slow but energy-efficient muscles.[25,29,30] According to previous studies, muscular energetic efficiency is inversely related to the shortening speed of the muscle.[31] Since tortoise muscles have a slow contraction speed, they possess high muscular efficiency. However, the slow muscles of the tortoise cannot quickly modify unwanted displacement, which can cause stability problems during walking. Tortoises solve this problem by selecting the appropriate gait.[32]

Another reason for the high efficiency of tortoises is the belly-dragging posture. Belly dragging reduces the load on each joint of the legs compared to locomotion without belly dragging by allowing part of the body to be supported on the ground and distributing the load.[33] In a similar manner, belly-dragging locomotion of tortoises distributes the load to reduce the load on the joints of legs and increases the load capacity.

Therefore, as mentioned earlier, we hypothesized that the energy efficiency of robots could be improved by leveraging the advantageous characteristics of the gait and belly-dragging posture of tortoises. To test this hypothesis, we designed a tortoise-like belly-dragging robot that can simulate the posture and gait of a tortoise. The design of the robot was inspired by the locomotion and plastron structure of tortoises, which were studied in prior zoological research. The tortoise-inspired robot is capable of six types of locomotion, consisting of different combinations of two gaits (diagonal and triangular) and three postures (one belly dragging and two nonbelly dragging).

We performed dynamic analyses to assess the general impact of tortoise-like locomotion on robot energy efficiency. To verify the broad applicability of our results, we varied parameters such as the robot's length, mass, friction coefficient of belly contact, and Froude number. In each simulation, the robot's CoT was measured and analyzed to determine changes in energy efficiency according to the locomotion strategy. To validate these findings from the simulations, real-world experiments were conducted with two varying conditions: payload and Froude number. The CoT was calculated by measuring the robot's power consumption and velocity. This approach allowed us to validate the simulation results against the experimental data and test the hypothesis regarding the energy efficiency of robot locomotion. In summary, the major contributions of this study are as follows. 1) Design of a quadrupedal robot capable of mimicking the belly dragging and gait of a tortoise and 2) theoretical and experimental confirmation of the hypothesis where imitating tortoise locomotion can enhance the energy efficiency of robots.

## 2. Design of Tortoise-Inspired Belly-Dragging Robot

### 2.1. Robot Design

The designed quadrupedal robot, as shown in **Figure 1**, imitates the tortoise's joint structure and sprawling posture. A 3D-printed plastron was attached to the bottom of the robot to perform belly dragging. The foot tips of the robot were made of ethylene–propylene diene monomer (EPDM). Other parts were designed via 3D computer-aided design (CAD) software (Inventor, Autodesk) and then printed on a 3D printer (M300 Plus, Zotrax). The 3D printing material used was high-impact polystyrene (HIPS); an acryl board with a thickness of 4 mm was used to increase the rigidity of the body. The robot had 12 servo motors (AX-12A 12, ROBOTIS) for locomotion, and a communication control board (OpenCM 485, ROBOTIS) for TTL communication of the motors was used between the motor and the controller. Total mass of the robot was about 1.806 kg, and it has dimensions of 370 mm width, 215 mm length, and 94 mm height. The lengths of the coxa, femur, and tibia forming the legs were 22.5, 67.5, and 75 mm, respectively.

### 2.2. Plastron Design

Turtles and tortoises have a shell structure that encloses the ventral and dorsal parts, protecting their internal organs. This shell, made of beta-keratin,[34] can be divided into two parts: the carapace, which covers the upper part, and the plastron, which covers the lower part. The plastron, a plate-like structure that protects the tortoise's belly, helps distribute the load on the ground during belly-dragging, aiding in efficient locomotion. However, belly dragging can have a negative impact on the animal's top speed and ability to maneuver due to constant contact and friction between the belly and the ground.[35] Therefore, to reduce the negative effects of belly dragging and increase energy efficiency, a plastron with a low coefficient of friction is needed.

In this study, six different 3D-printed plastrons were created to find a plastron with a low friction coefficient suitable for a tortoise-inspired robot. For five of them, the plastrons had the same flat structure, but were made of different materials including polylactic acid (PLA), HIPS, glycol-modified polyethylene terephthalate (PETG), polyurethane, and Nylon, as shown in Figure 1e. In addition, a patterned plastron was designed by engraving the macropattern of a real tortoise on the HIPS plastron, as shown in Figure 1f; this was based on a previous zoology study.[36] The plastrons were designed to be easily attachable and detachable to the robot. To select the plastron with the lowest friction coefficient suitable for the robot, experiments were conducted to measure the kinetic friction coefficient for each plastron, as detailed in Section 4.1.

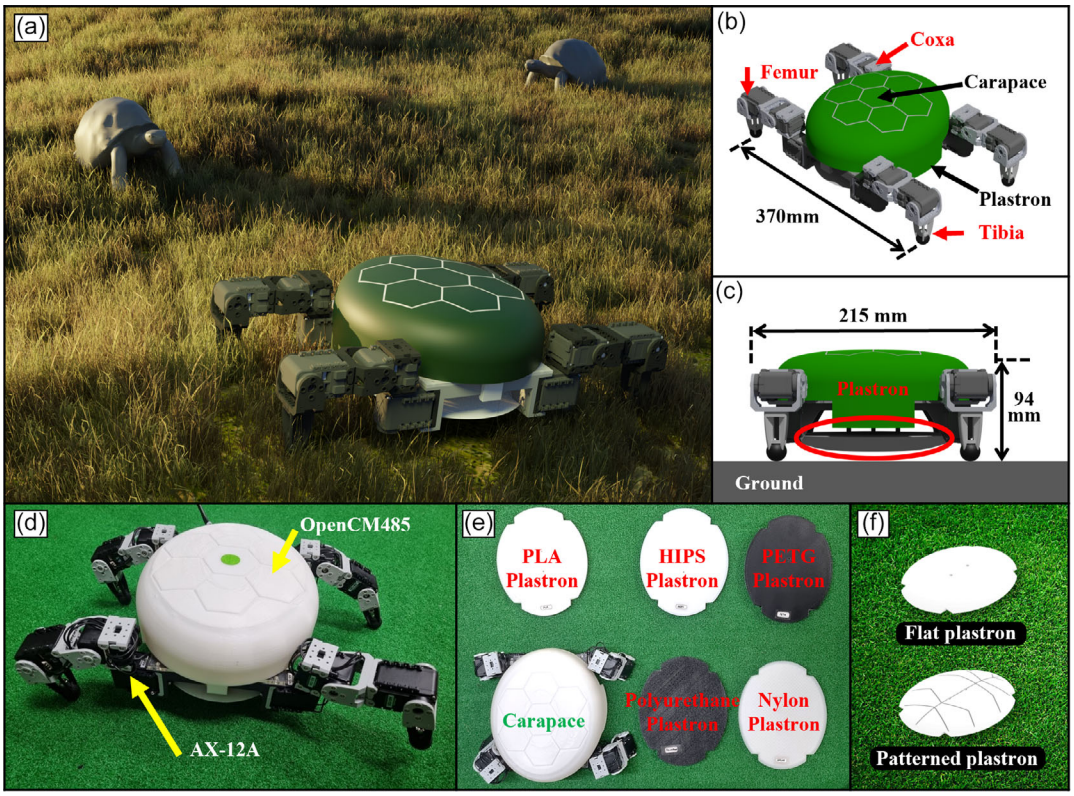


**Figure 1.** a) Tortoise-inspired belly-dragging robot. b) Schematic CAD design of tortoise-inspired belly-dragging robot. c) Side view of the robot. d) Tortoise-inspired belly-dragging robot with actuators (AX-12A) and extension board for TTL (OpenCM485). e) 3D-printed plastrons made of five different kinds of material. f) Flat and patterned plastron based on HIPS plastron.

### 2.3. Gait Design

Quadruped animals can be statically stable at all stages of locomotion by moving one leg at a time, keeping the center of gravity always above the triangle of support.[37] This stability is especially important for animals that cannot modify unwanted displacement quickly because of their slow muscles, and these animals should not lift the next foot until another foot touches the ground. However, despite having slow muscles, the tortoise employs a diagonal gait that supports the body with only two diagonal legs of the stride, using an unequal stride interval.[38,39]

This gait method of the tortoise serves to minimize unwanted displacement. Unwanted displacement occurs when the mean force applied to the body is not in equilibrium. In a previous study, researchers utilized Fourier series to model the ground forces during locomotion, distinguishing between walking and running through Fourier analysis.[40] Although the force record isn't inherently periodic, researchers treated it as part of an imagined periodic function to compute a Fourier series for its description. This approach allows for the expression of forces acting on the body during movement via Fourier series. In this case, if the velocity is slow enough, the force can be expressed only with the first term of the Fourier series and, under these conditions, the diagonal gait produces the smallest unwanted displacement at slow velocity.[41]

In this study, a triangular gait, which is commonly used by quadruped animals, and a diagonal gait, which is used by tortoises, were selected for comparison and applied to the tortoise-inspired belly-dragging robot. For convenience, individual legs are denoted as left forward (LF), right forward (RF), left hind (LH), and right hind (RH), as shown in **Figure 2**. Here, the stride length, cycle time, and swing percentage of the robot's triangular and diagonal gait were set to 0.09 m, 3 s, and 70%, respectively.

A triangular gait is an amble-like gait, in which the four legs move one by one. As shown in Figure 2a, the triangular gait moves in the order of LF → RH → RF → LH.

Mammals using an amble gait move their center of body (CoB) over a stable area created by ground contact points to overcome the stability problem caused by slow speeds. As the length of the stride increases, the possibility of the CoB deviating from the stable area increases, and CoB compensation is thus necessary. In a triangular gait with CoB compensation, three feet touch the ground in the swing phase to create a triangular stable area, and the robot's CoB thereby moves over the center of gravity of the stable area triangle. Figure 2c illustrates the process of a triangular gait with CoB compensation, starting from a stationary state.

A diagonal gait is a trot-like gait, in which a pair of diagonal legs move together. As shown in Figure 2b, the diagonal gait moves in the order of LH, RF → LF, RH → LH, RF → LF, RH and two feet touch the ground during the swing phase to create a straight stable area. The robot's CoB moves over this straight stable area. Figure 2d represents the process of the diagonal gait, starting from a stationary state.

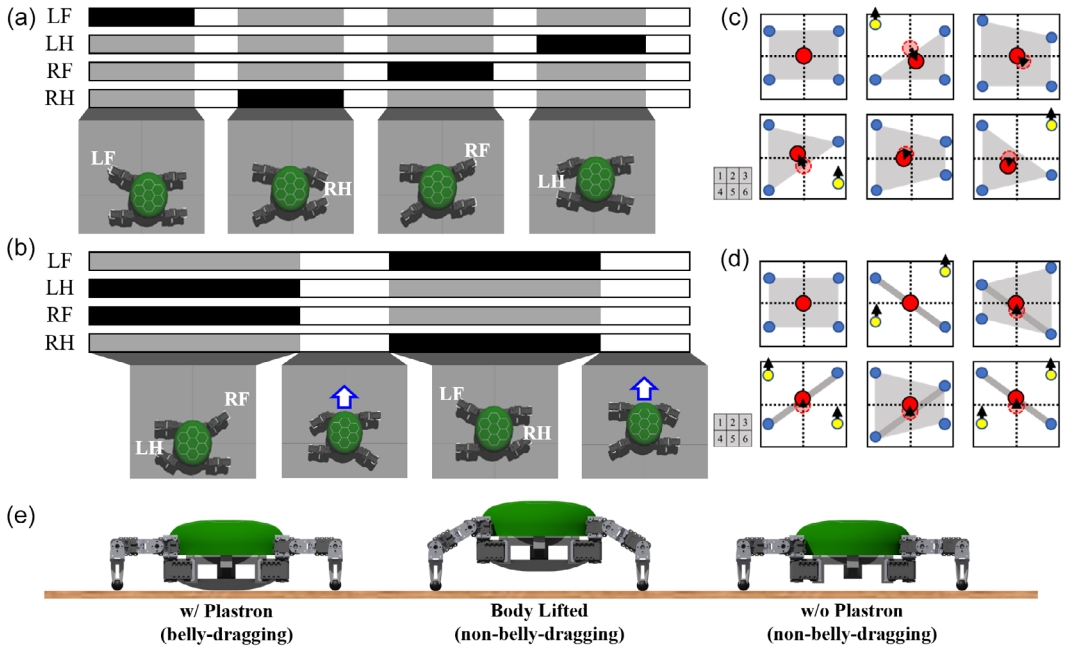


**Figure 2.** Gait design for tortoise-inspired belly-dragging robot. On the left, the black area is the swing phase, and the gray area is the stance phase. The white area represents the support phase. a) Triangular gait. b) Diagonal gait. On the right, red dots indicate the CoB, yellow dots represent legs in the swing phase, and blue dots are legs in the stance phase. The gray areas are stable areas. c) Triangular gait with CoB compensation. d) Diagonal gait with CoB compensation. e) Three different postures for robot locomotion.

In this study, the locomotion of the tortoise-inspired robot is represented by a combination of gaits and postures. Posture is an important factor in comparing the effectiveness of belly dragging with plastron. Therefore, in this study, for a fair comparison, we set up a total of three postures, as shown in Figure 2e. The first posture, "w/ Plastron," closely resembles the belly-dragging posture of a tortoise, with belly-dragging performed by the plastron. The second posture, "Body Lifted," involves elevating the robot's body with the plastron attached so that it does not employ belly dragging, and the robot's joint angles at rest differ from the case of "w/ Plastron." The third posture, "w/o Plastron," maintains the same joint angles at rest as those of "w/ Plastron," but without the use of belly dragging; this is achieved by removing the plastron from the robot. For convenience, we labeled individual postures as "w/ p" (with plastron), "lifted" (body lifted), and "w/o p" (without plastron). We conducted dynamic simulations and real-world experiments involving six locomotion combinations comprising these two gaits and three postures.

## 3. Dynamic Simulation

### 3.1. Preliminary Backgrounds

In the introduction, a hypothesis was proposed that applying the belly-dragging posture and gait of tortoises to a robot could enhance its energy efficiency. Forward dynamic simulations for various parameters were conducted to validate this hypothesis within a robot system, as shown in **Figure 3**a. The command values related to locomotion, such as gait type and locomotion velocity, serve as command parameters for the simulation. The gait controller in the dynamic simulation is composed of three elements: a gait generator, leg trajectory controllers, and a CoB compensator. The gait generator calculates the desired point ($x_d$) and gait phase ($\phi$) for each leg. Concurrently, the CoB compensator determines the CoB compensation ($\delta$), as detailed in Figure 2. Utilizing $x_d, \delta$, and $\phi$, the leg trajectory controllers solve the inverse kinematics problem and input the desired angle to the actuator controller.

For the dynamic simulation, Spatial_v2 library in the MATLAB R2021b Simulink environment was used.[42,43] Spatial_v2 utilizes a 6D spatial vector to calculate dynamics, offering a computational advantage over the existing 3D vector methods as it can simultaneously compute linear and angular physical quantities. Figure 3b illustrates one simulation environment using this library. In this environment, the dominant equation for the tortoise robot dynamics is Equation (1).

$$H(q)\ddot{q} + C(q,\dot{q}) = \tau + \sum_{k=1}^{N} J_k(q)^T \left(F_{k,n} + F_{k,t}\right) \tag{1}$$

where $H$, $C$, and $\tau$ respectively represent the mass-inertia matrix, the bias force including the gravitational and Coriolis forces, and the torque applied at the joint. $q$, $\dot{q}$, and $\ddot{q}$ indicate the angle, angular velocity, and angular acceleration of the robot's joints, respectively. $N$ is the number of contact points defined within the tortoise robot. By default, we set $N = 4$, considering all four legs, and increased it to $N = 5$ in cases in which belly contact occurred. $J_k(q)^T$ is the transpose of the Jacobian, which converts external forces applied on the tortoise robot into torque. $F_{k,n}$ and $F_{k,t}$ represent the normal and tangential forces applied at the $k^{\text{th}}$

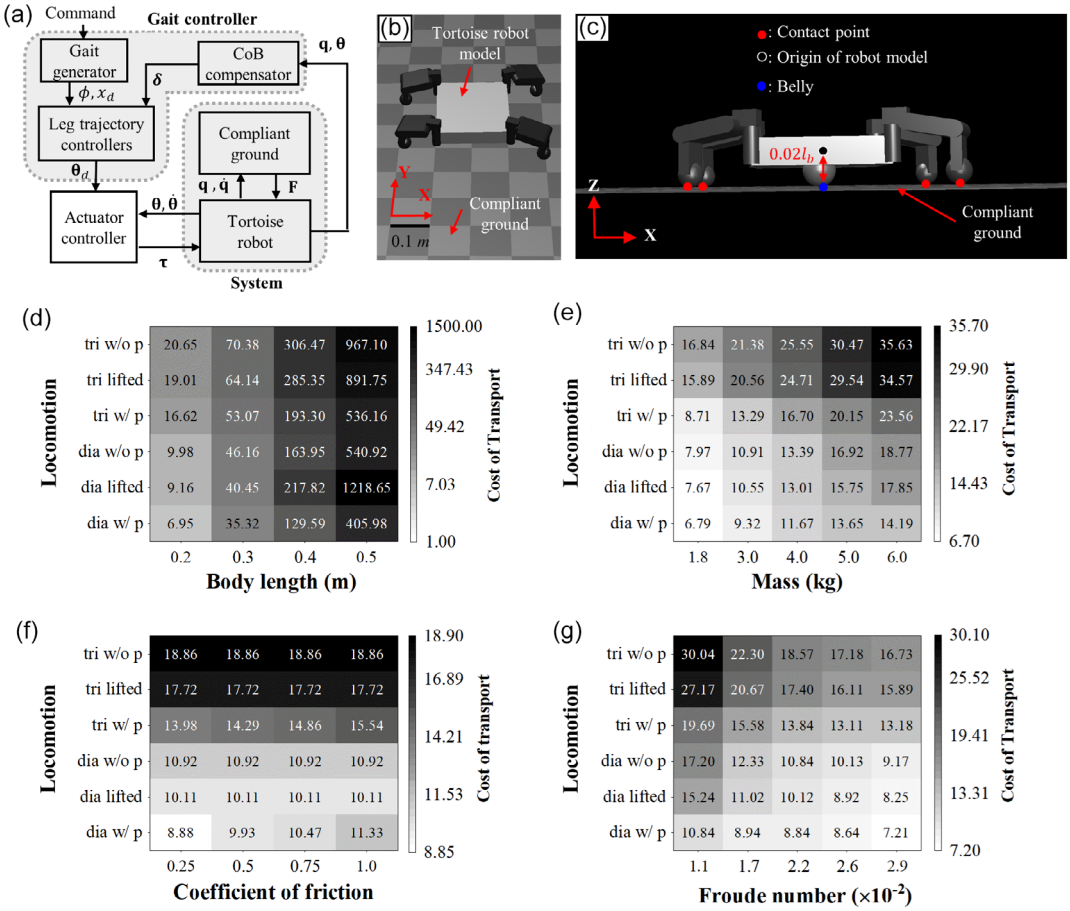


**Figure 3.** Settings and results of tortoise robot simulation. a) Schematic diagram of tortoise robot gait simulation, $\mathbf{q}$, $\dot{\mathbf{q}}$, $x_d$, $\phi$, $\delta$, $\theta$, $\theta_{\text{des}}$, $\tau$, and $\mathbf{F}$ represent the position, velocity, desired point, gait phase, CoB compensation, joint position, desired joint position, joint torque, and external force by contact, respectively. Bold and nonitalic symbols represent matrix components. b) Example of simulation environment, c) Contact points and origin of tortoise robot model. d) CoT results of body length simulation. The body mass values of the simulation model were 1.1, 3.7, 8.8, 17.2 kg as the body length increased from 0.2 to 0.5 m, respectively. e) CoT results of payload simulation. f) CoT results of coefficient of friction simulation. g) CoT results of Froude number simulation.

contact point. These forces are modeled using a compliant contact model, as shown in Equation (2) and (3).[44]

$$F_{k,n} = \begin{cases} K_n z_k^{\frac{3}{2}} + D_n z_k^{\frac{1}{2}} \dot{z}_k, & if\ z_k \le 0 \\ 0, & if\ z_k > 0 \end{cases} \tag{2}$$

$$F_{k,t} = \begin{cases} -\mu_k F_{k,n}, & if\ F_{k,\text{stick}} < -\mu F_{k,n} \\ \mu_k F_{k,n}, & if\ F_{k,\text{stick}} > \mu F_{k,n} \\ F_{k,\text{stick}} & otherwise \end{cases} \tag{3}$$

where $K_n$ and $D_n$ represent the spring coefficient and damper coefficient in the normal direction. $z_k$ and $\dot{z}_k$ are the $z$-axis displacement and velocity of the $k^{\text{th}}$ contact point, respectively. The exponents of $z_k$ multiplied after $K_n$ and $D_n$ are set to $\frac{3}{2}$ and $\frac{1}{2}$, respectively, based on another study.[45] $\mu_k$ is the friction coefficient of the $k^{\text{th}}$ contact point and is used to represent the friction coefficients for the belly and foot. In the context of the contact model, $F_{k,\text{stick}}$ denotes the stick friction acting on the $k^{\text{th}}$ contact point. This force functions as the tangential force, $F_{k,t}$, when it satisfies the friction cone constraint $-\mu_k F_{k,n} < F_{k,\text{stick}} < \mu_k F_{k,n}$. When this constraint is not met, slippage occurs, and the tangential force $F_{k,t}$ is instead set to $\mu_k F_{k,n}$ or $-\mu_k F_{k,n}$. $F_{k,\text{stick}}$ is defined as in Equation (4).

$$F_{k,\text{stick}} = -K_t d_k - D_t v_k \tag{4}$$

where $K_t$ and $D_t$ represent the spring and damping coefficients in the tangential direction. In the dynamic simulations, based on prior research, $K_t$ and $D_t$ are set to $K_n\sqrt{\max(0, -z)}$ and $D_n\sqrt{\max(0, -z)}$, respectively.[43] $d_k$ and $v_k$ denote the tangential elastic displacement and tangential velocity of the $k^{\text{th}}$ contact point, respectively.

In this study, we adopted values for the key parameters $K_n$ and $D_n$ in our compliant contact model based on previous research. In a study proposing the compliant normal force model in Equation (2), values of $K_n = 10^{10}\,\text{N m}^{-1}$ and $D_n = 10^5\,\text{Ns m}^{-1}$

were used to model the contact between a steel sphere and a cast iron plate.[45] On the other hand, another study modeling the contact between rubber and granite used a value of $K_n = 3.27 \times 10^5\,\mathrm{N\,m^{-1}}$.[46] Similarly, in a previous study modeling a medium surface, $K_n$ and $D_n$ were set at $3 \times 10^5\,\mathrm{N\,m^{-1}}$ and $700\,\mathrm{Ns\,m^{-1}}$, respectively.[47] To implement compliant ground contact for the tortoise robot in an experimental environment similar to those in previous research,[46,47] we combined the values used in those studies and set $K_n = 3 \times 10^5\,\mathrm{N\,m^{-1}}$ and $D_n = 700\,\mathrm{Ns\,m^{-1}}$.

The parameters that vary according to the simulation cases in **Table 1** include the robot's length, mass, belly friction coefficient, and Froude number. These parameters directly impact the robot's shape and behavior. Changes in the system's mass, velocity, and gait cycle due to these parameters were modeled using equations such as Equation (5)–(8), which provide formulations for geometric similarity, dynamic similarity, stride frequency, and stride length.

Geometric similarity is a concept that exists when the body dimensions of animals with different sizes satisfy Equation (5).[48] This concept can be applied to determine factors such as the size of robots.[49,50] In Simulation I in this study, the change in body mass as a function of body length was calculated using Equation (5).

$$l_b = a m_b^{0.333} \tag{5}$$

where $l_b$ and $m_b$ represent the robot's body length and body mass, respectively, and $a$ is a constant for geometric similarity, determined based on values used in robot design and gait design. The exponent of $m_b$ was set to 0.333, assuming that, as the volume of the robot increases, its mass increases proportionally.

Dynamic similarity is a concept proposed to generalize the behaviors of animals of different sizes. Equation (6) is related to the Froude number $b$ and is used to determine dynamic similarity. Dynamic similarity occurs when one motion is identical to another motion when lengths, times, and forces are multiplied by specific factors ($\lambda$, $\tau$, and $\phi$).[48] To maintain dynamic similarity, velocities and accelerations must be scaled by $\lambda/\tau$ and $\lambda/\tau^2$, respectively. Applying Newton's second law, masses should be multiplied by $\phi\lambda/(\lambda/\tau)^2$ to maintain this similarity. That is, the mass ratio, derived from the ratio of forces, lengths, and velocities, simplifies to a fundamental expression: $(\text{Ratio of masses} * (\text{Ratio of velocities})^2)/(\text{Ratio of forces} * \text{Ratio of lengths}) = 1$. Consequently, dynamically similar motions share a common $mv^2/Fl$ value. In contexts where gravitational force ($F = mg$) is important, like in locomotion, this equivalence translates to $v^2/gl = b^2$. Hence, if two different animals exhibit the same Froude number $b$ in their actions, their behaviors are considered dynamically similar. Although the Froude number originates from biological concepts, it is widely applied to robots using gaits as well.[51] In Simulation I of this study, the velocity was set to maintain dynamic similarity even when body length changed. In Simulation IV, different locomotion velocities with distinct Froude numbers were applied to Tortoise robots of the same size.

**Table 1.** Parameters according to simulation case.

| Simulation case | I | II | III | IV |
|---|---|---|---|---|
| Parameter | Body length [m] | Robot mass [kg] | CoF on belly | Froude number |
| 1 | 0.2 | 1.8 | 0.25 | $1.1 \times 10^{-2}$ |
| 2 | 0.3 | 3.0 | 0.50 | $1.7 \times 10^{-2}$ |
| 3 | 0.4 | 4.0 | 0.75 | $2.2 \times 10^{-2}$ |
| 4 | 0.5 | 5.0 | 1.00 | $2.6 \times 10^{-2}$ |
| 5 | – | 6.0 | – | $2.9 \times 10^{-2}$ |

$$\sqrt{\frac{v^2}{gl_b}} = b \tag{6}$$

where $v$, $g$, and $l_b$ represent the robot's locomotion velocity, gravitational acceleration, and body length, respectively. $b$ is the Froude number; the default Froude numbers in Simulations I, II, and III were determined based on values used in robot design and gait design.

Stride frequency refers to the number of strides performed in a unit of time. When performing the same action, even for similar species of animals, as the size of the individual increases, the stride length becomes longer, and the stride frequency decreases.[48] Equation (7) is the formula for calculating stride frequency $f$ within the simulation.

$$f = \frac{1}{T} = c m_b^{-0.13} \tag{7}$$

where $f$, $T$, and $m_b$ respectively represent the stride frequency of the gait, the period of the gait, and the robot's body mass. $c$ is a constant for stride frequency, determined based on values used in robot design and gait design. The exponent of $-0.13$ used in Equation (7) was determined by applying the trend in stride frequency exhibited by the ornate box turtle, a species of terrestrial turtle.[52] This value is an exponent obtained from regression analysis of stride frequency based on the masses of 33 ornate box turtles.

Equation (8) is the formula used to determine the stride length and leg stroke in the gait, based on the locomotion velocity $v$.

$$\lambda = vT = \frac{R}{\beta} \tag{8}$$

where $\lambda$, $v$, $T$, $R$, and $\beta$ represent the stride length of the gait, the locomotion velocity of the robot, the cycle time of the gait, the leg stroke, and the duty factor, respectively.

Triangular and diagonal gaits are both symmetrical gaits in which individual legs follow identical trajectories. Therefore, each gait is characterized by a single cycle time, leg stroke, and duty factor. The duty factor represents the proportion of time one foot is in contact with the ground during a single gait cycle, while leg stroke signifies the distance one foot moves during one complete gait cycle.[53] Equation (9) and (10) are used to calculate the duty factor and leg swing ratio within the simulation.

$$\beta = 1 - \alpha r_l \tag{9}$$

$$\alpha = \begin{cases} 0.25, & \text{if triangular gait} \\ 0.5, & \text{if diagonal gait} \end{cases} \tag{10}$$

where $\alpha$ and $r_l$ represent the duty factor and leg swing ratio of the gait, respectively. In this study, $r_l$ was set to 70%, and $\alpha$ was determined by Equation (10). According to Equation (9), the duty factors for the diagonal gait and triangular gait were set to 0.65 and 0.825, respectively.

### 3.2. Setup for Dynamic Simulation

Analysis of CoT in the simulation was performed for a single gait cycle, and CoT was calculated using Equation (11).

$$(\text{CoT}) = \frac{1}{mgd}\sum_{j=1}^{N}\sum_{i=1}^{12}\left(|\tau_{i,j}\omega_{i,j}| + 7.4\tau_{i,j}^2\right)h_j \tag{11}$$

where $m$, $g$, and $d$ represent the total mass of the robot, gravitational acceleration, and robot's locomotion distance, respectively. $\tau_{i,j}$ and $\omega_{i,j}$ denote the torque and angular velocities applied to the $i^{\text{th}}$ joint at the $j^{\text{th}}$ time step, respectively. $h_j$ is the $j^{\text{th}}$ time step size of the simulation. The coefficient of 7.4 in front of $\tau_{i,j}^2$ is calculated considering account motor specifications; the derivation of this term is covered in the Supporting Information.

A total of four different simulations were conducted to determine whether the gait characteristics of tortoises can be generalized to robotic systems. In each simulation, we considered two types of gait (triangular and diagonal gait) and three postures ("w/ p," "w/o p," and "lifted"), resulting in a total of six types of locomotion. The parameters that were varied in the four simulations are specified in Table 1.

In Simulation I, the objective was to investigate the CoT of locomotion for the tortoise robot with respect to variations in its size. For this purpose, a range of body lengths was considered, and the corresponding body mass was determined using Equation (5). Additionally, to maintain dynamic similarity, the locomotion velocity was calculated as a function of body length through Equation (6). Stride frequency was determined as a function of body mass using Equation (7).

In Simulation II, the objective was to examine the CoT of the tortoise robot in relation to different payloads. For this objective, scenarios with various payloads on tortoise robot with a fixed body length of 0.2 m were considered. In this context, parameters other than the mass of the tortoise robot were maintained constant using Equation (6) and (7), and CoT was subsequently analyzed.

In Simulation III, the objective was to assess the influence of the friction coefficient acting on the belly of the tortoise robot on the CoT during locomotion. For this objective, scenarios with various friction coefficients of a robot belly with a fixed body length of 0.2 m were considered.

In Simulation IV, the objective was to investigate the CoT of the tortoise robot based on the Froude number of the locomotion. For this objective, scenarios with various Froude numbers with fixed body length of 0.2 m were considered.

In all simulations except for Simulation III, which considered the friction coefficient of the belly as a variable, the friction coefficient of the belly was set to the lowest value among the values in Table 1, which is 0.25. For all simulations, the friction coefficient at the foot tip was set to 1.0. Additionally, in all simulations except for Simulation IV, which focuses on dynamic similarity, the Froude number was set to the middle value in Table 1, which is $2.2 \times 10^{-2}$.

In Simulations II, III, and IV, the body length was fixed at 0.2 m, and other parameters such as link masses, link lengths, and offset were set to specific values. The reference masses for the coxa, femur, and tibia links were 0.072, 0.074, and 0.018 kg, respectively. The lengths of these links were 0.0236, 0.0710, and 0.075 m, respectively. The $z$-axis link offset for the Coxa link was 0.0378 m. In simulation I, these parameters were used as references, and the mass and length were scaled by factors $\frac{m_b}{m_{b,0}}$ and $\frac{l_b}{l_{b,0}}$, respectively. Here, $m_b$, $l_b$, $m_{b,0}$, and $l_{b,0}$ respectively represent body mass, body length, reference body mass (1.1 kg), and reference body length (0.2 m).

The gaits in this article assume a constant body height of the robot. In the case of belly dragging, the pattern of ground reaction forces (GRF) may change depending on the body height of the gait, which may lead to interference with locomotion. Therefore, selecting an appropriate body height that does not interfere with locomotion is crucial, especially in the case of belly-dragging locomotion.

Simulations were performed for various body heights to determine an appropriate value. For each gait, a body height was selected for which the GRF applied to the belly was equal to or less than the GRF applied to the foot. The results of the dynamic simulations using the selected body height are discussed in Section 3.3, and the metrics such as CoT, torque, and velocity, observed during the body height selection process, are discussed in Section 5.2.

The ODE15s solver was used to simulate compliant contact, and the relative tolerance for the simulation was set to $10^{-3}$.

To implement actuators in the simulation similar to those used in the tortoise robot, an additional controller was designed. This controller, as depicted in Figure 3a, was named the "actuator controller." Within this controller block, parameters such as the compliant margin, which determines the extent of toleration of errors based on the robot's specifications, and the compliant slope, which is similar to the P-gain, as well as torque limitations due to motor stall torque, were implemented. Detailed explanations of this controller are provided in the Supporting Information. The maximum torque of the actuator in simulations was set as Equation (12) based on the body length and the stall torque of the actual robot, which is 1.5 Nm.

$$\tau_{\text{stall}} = 1.5\frac{m_b l_b^2}{m_{b,0} l_{b,0}^2} \tag{12}$$

where $m_b$ and $l_b$ represent the body mass and length of the tortoise robot. $m_{b,0}$ and $l_{b,0}$ are the reference body mass and length of the tortoise robot within the simulation, set to 1.1 kg and 0.2 m, respectively.

In the simulation, the body height $z_h$ was adjusted proportionally to the body length using Equation (13).

$$z_h = 0.257 l_b + \frac{l_b}{l_{b,0}} G \tag{13}$$

where $z_h$, $l_b$, $l_{b,0}$, and $G$ represent the $z$-axis distance from the origin of the robot model to the contact point of the foot, the body length, the reference body length (0.2 m), and an offset for adjusting the body height, respectively. The $z$-axis distance from the origin of the robot model to the contact point of the belly was $0.257l_b$. To ensure that the body height increased proportionally with the increase in the body length, $\frac{l_b}{l_{b,0}}$ was multiplied by the offset $G$. As shown in Figure 3c, the ground contact points of the tortoise robot are represented as red and blue circles. The $z$-axis distance from the origin to the blue dot remains constant within the simulation robot model, and the $z$-axis distance from the origin to the red dot is determined by $z_h$.

### 3.3. Dynamic Simulation Result

#### 3.3.1. Simulation Results with Varying Body Lengths

Figure 3d shows results of Simulation I, which investigated the CoT as a function of robot body length. The "dia w/ p" posture consistently had a lower CoT than the "dia w/o p" posture, with the largest difference of 30.43% observed at a body length of 0.2 m. Similarly, the "dia w/ p" posture consistently had a lower CoT than the "lifted" posture, with the largest difference of 66.69% observed at a body length of 0.5 m. These results indicate that the "w/ p" posture consistently shows the lowest CoT when using a diagonal gait, regardless of body length.

"tri w/ p" consistently had a lower CoT than "tri w/o p" and "tri lifted," with largest differences of 44.56% and 39.88%, respectively, observed at a body length of 0.5 m. Similar to the diagonal gait, the "w/ p" posture consistently showed the lowest CoT in the triangular gait, regardless of body length.

When both the triangular gait and diagonal gait adopted the "w/ p" posture, the diagonal gait consistently had a lower CoT than the triangular gait. The difference in CoT between these two gaits with the "w/ p" posture was largest at a body length of 0.2 m, where "dia w/ p" had a 58.20% lower CoT than "tri w/ p." In summary, for Simulation I, the locomotion with the lowest CoT, regardless of body length, was the one that performed belly-dragging and diagonal gait, referred to as "dia w/ p."

#### 3.3.2. Simulation Results with Varying Payloads

Figure 3e shows the results of Simulation II, which examined the CoT with varying payloads for the tortoise robot. When using the diagonal gait, the "w/ p" posture consistently had a lower CoT than other postures, regardless of robot mass. In particular, at a robot mass of 6.0 kg, the "w/ p" posture showed the largest difference compared to the "w/o p" and "lifted" postures, with CoT reductions of 24.42% and 20.54%, respectively.

In the case of using the triangular gait, the "w/ p" posture also consistently had a lower CoT than the other postures, regardless of robot mass. At a robot mass of 1.8 kg, the "w/ p" posture showed the largest difference compared to the "w/o p" and "lifted" postures, with CoT reductions of 48.29% and 45.20%, respectively. These results confirm that the "w/ p" posture is the most energy-efficient type of locomotion for both gaits, regardless of body mass.

With the same "w/ p" posture, the diagonal gait consistently showed a lower CoT than the triangular gait. The difference in CoT between these two gaits was most significant when the robot's mass was the largest at 6 kg, with "dia w/ p" having a 39.79% lower CoT than "tri w/ p." Therefore, similar to the results of Simulation I, the locomotion with the lowest CoT in Simulation II was "dia w/ p," regardless of the robot's mass.

#### 3.3.3. Simulation Results with Varying Belly's Coefficients of Friction

Figure 3f shows the results of Simulation III, which investigated the effect of the friction coefficient applied to the tortoise robot's belly on CoT. Changes in the friction coefficient applied to the robot's belly only affected the "w/ p" posture, using which the robot performed belly dragging. When the friction coefficient was less than 0.75, "dia w/ p" showed a lower CoT than "dia lifted," with the most significant difference of 12.11% observed at the lowest friction coefficient of 0.25. However, when the friction coefficients of the belly were 0.75 and 1.00, "dia w/ p" showed a higher CoT than "dia lifted," with the most significant difference of 12.08% observed at the highest friction coefficient of 1.00. Similarly, when the friction coefficient was less than 1.00, "dia w/ p" showed a lower CoT than "dia w/o p," with the most significant difference of 18.63% observed at the lowest friction coefficient of 0.25. At the friction coefficient of 1.00, "dia w/ p" showed a 3.76% higher CoT than "dia w/o p." In summary, "dia w/ p" showed the lowest CoT when the friction coefficient of the belly was less than 0.75, with lower friction coefficients resulting in lower CoT.

For the triangular gait, the "w/ p" posture consistently showed a lower CoT regardless of the friction coefficient applied to the belly. The CoT difference of "tri w/ p" compared to "tri w/o p" and "tri lifted" was most significant when the belly friction coefficient was 0.25, with differences of 25.85% and 21.10%, respectively. These results differ from the diagonal gait results, as the "w/ p" posture showed the lowest CoT even when the belly friction coefficient was greater than 0.75. However, the commonality between both results is that lower belly friction coefficients led to lower CoT. Therefore, it can be concluded that a lower belly friction coefficient can increase the energy efficiency of the "w/ p" posture.

With the same "w/ p" posture, similar to Simulations I and II, the diagonal gait consistently showed a lower CoT than the triangular gait. The CoT difference between the two gaits with the "w/ p" posture was most significant when the friction coefficient of the belly was 0.25. In this case, "dia w/ p" had a CoT that was 36.47% lower than that of "tri w/ p." Therefore, assuming a low belly friction coefficient, the locomotion with the lowest CoT in Simulation III was "dia w/ p."

#### 3.3.4. Simulation Results with Varying Froude Numbers

Figure 3g shows the results of Simulation IV, in which the CoT was analyzed based on the Froude number. The changes in Froude number correspond to changes in dynamic similarity,

described earlier. When using the same gait, the "w/ p" posture showed the lowest CoT even if the Froude number of the gait changed. "dia w/ p" consistently had lower CoT than "dia w/o p" and "dia lifted," with the most significant differences occurring when the Froude number was $1.1 \times 10^{-2}$, showing differences of 36.93% and 28.86%, respectively. Similarly, "tri w/ p" consistently showed lower CoT than "tri w/o p" and "tri lifted," with the most significant differences of 34.44% and 27.53%, respectively, at a Froude number of $1.1 \times 10^{-2}$. When comparing the two gaits, the diagonal gait consistently showed lower CoT. The difference between the two gaits with "w/ p" posture was greatest at a Froude number of $2.9 \times 10^{-2}$, with "dia w/ p" having a CoT 45.30% lower than that of "tri w/ p." Therefore, regardless of the Froude number, the locomotion with the lowest CoT in Simulation IV was "dia w/ p."

The simulation results confirm that implementing belly dragging with the "w/ p" posture can increase the energy efficiency of locomotion for tortoise robots. Particularly, when performing belly dragging, diagonal gait tends to exhibit higher locomotion efficiency than triangular gait. Additionally, as assumed in the robot design in Section 2, a lower friction coefficient applied to the tortoise robot's belly contributes to more efficient belly-dragging locomotion. Based on these findings, it is evident that regardless of changes in parameters such as body length, mass, belly friction coefficient, and Froude number, locomotion with belly-dragging and diagonal gait ("dia w/ p" locomotion) consistently exhibits the lowest CoT. The reasons behind the differences in CoT based on posture and gait, as well as why "dia w/ p" locomotion achieves the highest efficiency, will be discussed in Section 5.

## 4. Locomotion Experiment

Dynamic simulations offer the advantage of exploring results for various variables that may be challenging to replicate in real-world experiments. However, it's crucial to verify experimentally if the results obtained from these simulations are also observable in actual robots. To bridge this gap between simulation and reality, real-world locomotion experiments were conducted. This approach allows for a comprehensive validation of the findings, demonstrating the practical applicability of the simulated scenarios.

From the results of the dynamic simulations, it was confirmed that a lower coefficient of friction in the belly reduces the CoT (Simulation III). Additionally, it was observed that the tortoise's locomotion ("dia w/ p") consistently showed the lowest CoT, even under varying conditions of body length, payload, and Froude number (Simulation I, II, IV). To verify this in actual robots, locomotion experiments were conducted with the robot designed as per Section 2.1, featuring a fixed body length. Initially, based on the results of Simulation III, an experiment was conducted to select a plastron with the lowest coefficient of friction (Section 4.1). Additionally, experiments were conducted to determine whether the tortoise's locomotion is the most efficient, similar to the results of Simulation II and IV, regardless of the payload or Froude number (Section 4.3).

### 4.1. Plastron Selection

In Section 3.3, it was confirmed that the plastron should have a low coefficient of friction to achieve low CoT. To select the plastron for the robot locomotion experiment, an experiment was conducted to measure the coefficient of kinetic friction on the six designed plastrons, as shown in Figure 1. The friction measurement experiment was carried out on a wooden board and a grass mat, target environments for the locomotion experiment, as described later in Section 4.2. As shown in **Figure 4**a, the plastron was dragged across the driving terrain using a linear stage, and the friction force was measured using a load cell (BCL-3L, CAS). The friction coefficient was calculated by dividing the measured friction force by the normal force, which was generated by the combined weight of the plastron and an additional 1 kg weight. The linear stage was actuated at an initial acceleration of $10\,\mathrm{cm\,s^{-2}}$ and a velocity of $5\,\mathrm{cm\,s^{-1}}$ for 20 s, with five repeats of each experiment. To obtain an accurate kinetic friction coefficient that excludes the effects of static friction, the measurements were performed by averaging the data between 2.5 and 10 s after the plastron started to drag. The start of the measurement interval (2.5 s) was experimentally determined by observing the voltage of the load cell; this starting moment was when the effect of static friction disappeared.

Figure 4b shows results of measuring the friction coefficient of the six plastrons. First, kinetic friction coefficients of the plastron with and without patterns were measured. Patterns in an animal's integument or exoskeleton, such as the scales of a snake, often affect its friction properties. In this experiment, we aimed to determine the effect of macroscopic patterns on the friction coefficient of a tortoise's plastron and to determine which form, flat or patterned, has a lower friction coefficient. As shown in the comparison between the HIPS and Patterned HIPS plastrons, the flat plastron had a lower kinetic friction coefficient than the patterned plastron on both the wooden board and the grass mat. These results confirm that the flat plastron has a lower coefficient of friction.

The second experiment measured the kinetic friction coefficient of the plastron according to the material. In this experiment, five different plastron materials with flat shape, selected from the first experiment, were used. Among the five different materials of the flat plastron, the PLA plastron had the lowest friction coefficient, with an average value of 0.228 on the wooden board and 0.261 on the grass mat. Based on these results, a flat plastron made of PLA was chosen for the locomotion experiment.

### 4.2. Experimental Setup

The experimental conditions for the locomotion experiment are shown in Figure 4c; these included two different environments and two different robot masses. The first environment was a flat, polished wooden board; the second was a grass mat with higher friction and uneven contact characteristics. For the case of the robot's increased payload, a total of 0.4 kg (0.2 kg + 0.2 kg) of weights were attached to the carapace. Given that the robot's mass is 1.806 kg, the original and increased masses of the robot are denoted as 1.8 and 2.2 kg, respectively.

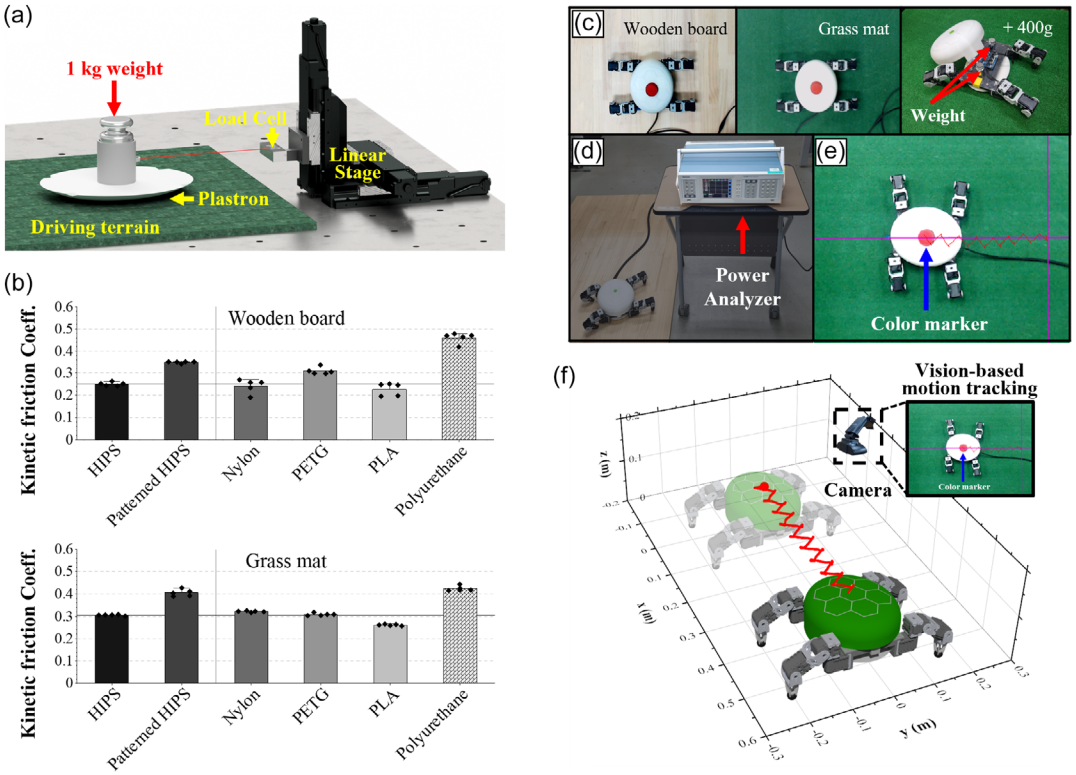


**Figure 4.** Experimental setup for measuring the designed plastrons' kinetic friction coefficient and the power consumption and velocity of the robot. a) Experimental setup using a load cell and linear stage. b) Kinetic friction coefficient according to materials of plastron. The reference lines represent the kinetic friction coefficient of the HIPS flat plastron. c) Tortoise-inspired robot on wooden board and grass mat environment and locations of weights on robot for increased payload. d) Setup for measuring power consumption using a power analyzer (PA3000 and BB1000-EU, Tektronix). e) Setup for vision-based analysis tool (Tracker, Open source physics) with a color marker. f) Schematic for measuring the trajectory and velocity of the robot using a vision-based analysis tool.

For the experiment with varying payloads, the Froude number was consistently maintained at $2.2 \times 10^{-2}$, while the mass and driving environment were varied. Thus, four different combinations of experimental conditions were tested in the first experiment, which included two robot masses (weight loaded and unloaded) and two different material environments. For the experiment with varying Froude numbers, the mass was fixed at 1.8 kg and the driving environment was a wooden board, whereas the target velocity of the robot was varied. Froude numbers of $1.1 \times 10^{-2}$, $2.2 \times 10^{-2}$, $2.9 \times 10^{-2}$ were used, and the target velocity was determined based on the Froude number. Thus, three different experimental conditions were tested in the second experiment.

We used the CoT of the robot to compare the locomotion efficiency of the robot according to the presence or absence of belly dragging in the gait. CoT can be expressed as Equation (14) below.

$$(\mathrm{CoT}) = \frac{Work(J)}{mg\lambda(kg \times m^2/s^2)} = \frac{P(J/s) \times t(s)}{mg(kg \times m/s^2) \times v(m/s) \times t(s)} \quad (14)$$

where $P$ denotes the power consumed by the robot, $t$ is the travel time (s), $m$ is the mass (kg), $g$ is the gravitational acceleration ($\mathrm{m\,s^{-2}}$), and $v$ represents the velocity of the robot ($\mathrm{m\,s^{-2}}$). Therefore, to calculate the CoT, the velocity and power consumption need to be measured.

To measure the power consumption during robot locomotion, a power analyzer (PA3000 and BB1000-EU, Tektronix) was used, as shown in Figure 4d. The power consumption was obtained by averaging the measured electrical input power during the locomotion, which is measured in watts. Also, after attaching a color marker to the robot, the trajectory, velocity, and travel time were measured using a vision-based analysis tool (Tracker, Open source physics), as shown in Figure 4e,f. The experiment was configured to measure the power consumption, velocity, and travel time of the robot simultaneously, and experiments were repeated five times for each of the four environments and six types of locomotion.

Measurement of the experimental results started when the robot started locomotion and ended when it reached the target point at a distance of about 40 cm. For each type of locomotion, the velocity was measured in $\mathrm{m\,s^{-1}}$ from the start to the end of the locomotion.

### 4.3. Locomotion Experiment Result

As mentioned in Section 4.2, experiments with varying payloads were conducted on two different types of surface (wooden board, grass mat), resulting in a total of four experimental conditions. Experiments with varying Froude numbers were conducted on wooden board with the original robot mass, resulting in a total of three experimental conditions. For each experiment, the velocity and power consumption were measured to calculate the CoT.

#### *4.3.1. Experiment Results with Varying Payloads*

**Figure 5**a shows the measured velocities of the robot in experiment with varying payloads. Despite implementing the same stride length, cycle time, and swing percentage, the velocity of the robot was found to differ depending on experimental conditions and type of locomotion. This is due to factors such as foot tip slip and belly dragging, which were not considered in the locomotion planning. While the robot's foot tip moves along the desired trajectory kinematically, its locomotion in a real environment is hindered by these factors.

Power consumption measurement results of the six types of locomotion for the four experimental conditions are shown in Figure 5b,c. Compared to the other postures, the "w/ p" posture with belly dragging led to smaller power consumption for both 1.8 and 2.2 kg robots traveling on wooden boards and grass mats. When using the same gait, the "lifted" posture consistently resulted in the highest power consumption, regardless of the robot's payload or the driving environment. Additionally, the diagonal gait had lower power consumption compared to the triangular gait, when the postures were the same.

In general, "diagonal w/ p" had the lowest power consumption and "triangular lifted" had the highest power consumption in all four experimental conditions (1.8 and 2.2 kg payload on wooden board and 1.8 and 2.2 kg payload on grass mat environment). Numerically, "diagonal w/ p" showed power consumption reductions of 32.341%, 39.044%, 40.123%, and 47.304% in the above four conditions compared to those values of the "triangular lifted," respectively.

The results of the CoT using Equation (14) with measured power consumption, velocity, and mass of the robot are shown in Figure 5d,e. Similar to power consumption, the "w/ p" posture with belly dragging had the lowest CoT in all four experimental conditions, and the "lifted" posture had the highest CoT when

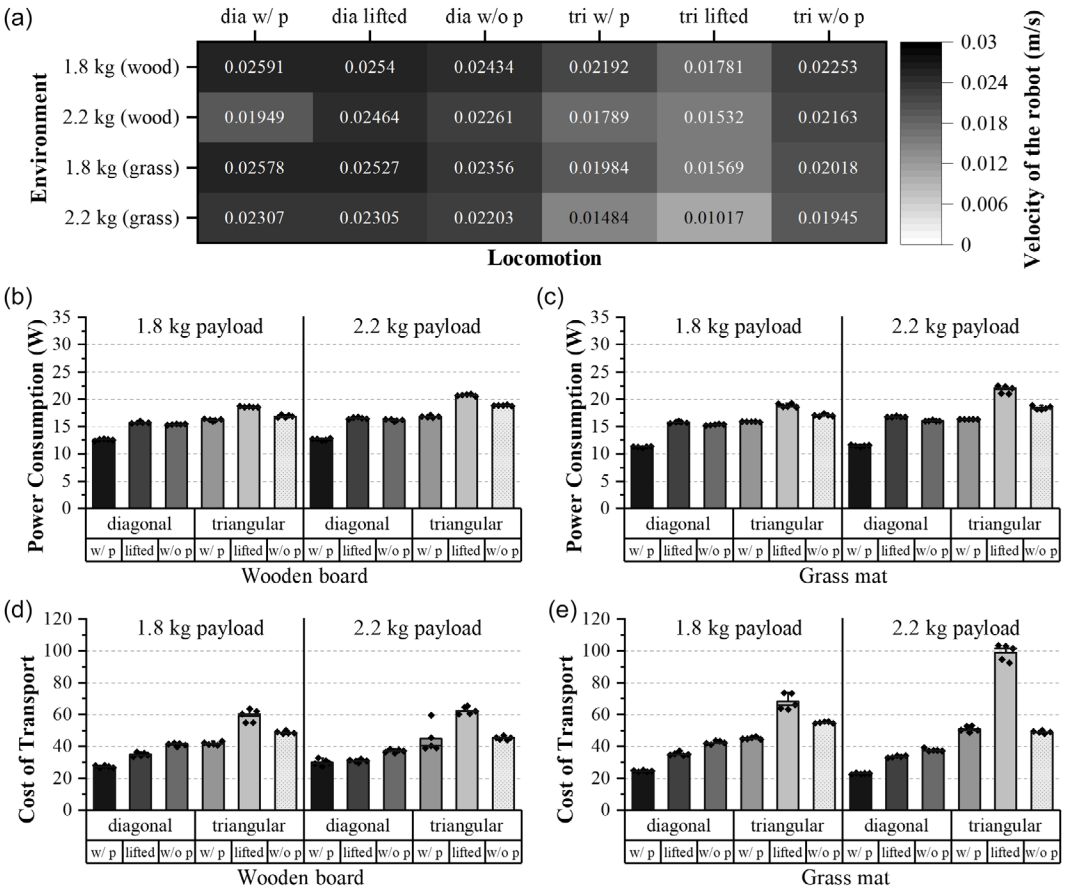


**Figure 5.** Results of the locomotion experiment with varying payloads. a) The average velocities of the robot. b,c) Power consumption of the robot according to the gait and posture in the wooden board and grass mat, respectively. d,e) The robot's transport cost according to the gait and posture in the wooden board and grass mat environment, respectively.

using the triangular gait. However, when using the diagonal gait, the "w/o plastron" posture had the largest CoT, while "lifted" posture had the largest power consumption. On the other hand, CoT according to gait was lower for diagonal gait than for triangular gait regardless of posture, robot mass, and driving environment.

In general, "diagonal w/ p" had the lowest CoT in varying payloads and environment conditions, while "triangular lifted" has the highest value. Numerically, "diagonal w/ p" had 53.650%, 51.948%, 63.676%, and 76.794% lower values of CoT than those of "triangular lifted," respectively, in the four conditions.

#### 4.3.2. Results of Varying Froude Numbers

**Figure 6**a shows the average velocities of the robot in experiment with varying Froude numbers. Since the target velocity is determined based on Equation (6), a higher Froude number condition resulted in a higher velocity of the robot.

Power consumption measurement results for the three Froude number conditions are shown in Figure 6b. The results showed similar tendency to the results of Section 4.3.1. The "w/ p" posture with belly dragging led to smaller power consumption for every Froude number conditions compared to the other postures. When using the same gait, the "lifted" posture consistently showed the highest power consumption, regardless of the Froude number. When the postures were the same, the diagonal gait had lower power consumption compared to the triangular gait.

Generally, "diagonal w/ p" had the lowest power consumption, while "triangular lifted" had the highest power consumption across all Froude number conditions. Numerically, compared to those values of the "triangular lifted," "diagonal w/ p" showed reductions in power consumption of 41.750%, 32.341%, and 29.640% in the three Froude number conditions, listed in increasing order, respectively.

The calculated results of the CoT, using Equation (14) which takes into account the measured power consumption, velocity, and mass of the robot, are presented in Figure 6c. It was observed that, in varying Froude number conditions, the "w/ p" posture for each gait generally exhibited the lowest CoT compared to other postures, with the exception of the triangular gait at a Froude number of $2.9 \times 10^{-2}$. Considering that the "tri w/ p" had lower power consumption than "tri lifted" in this Froude number condition and that "tri w/ p" demonstrated slower speeds, this exception can be attributed to unexpected locomotion hindrances caused by belly dragging. On the other hand,

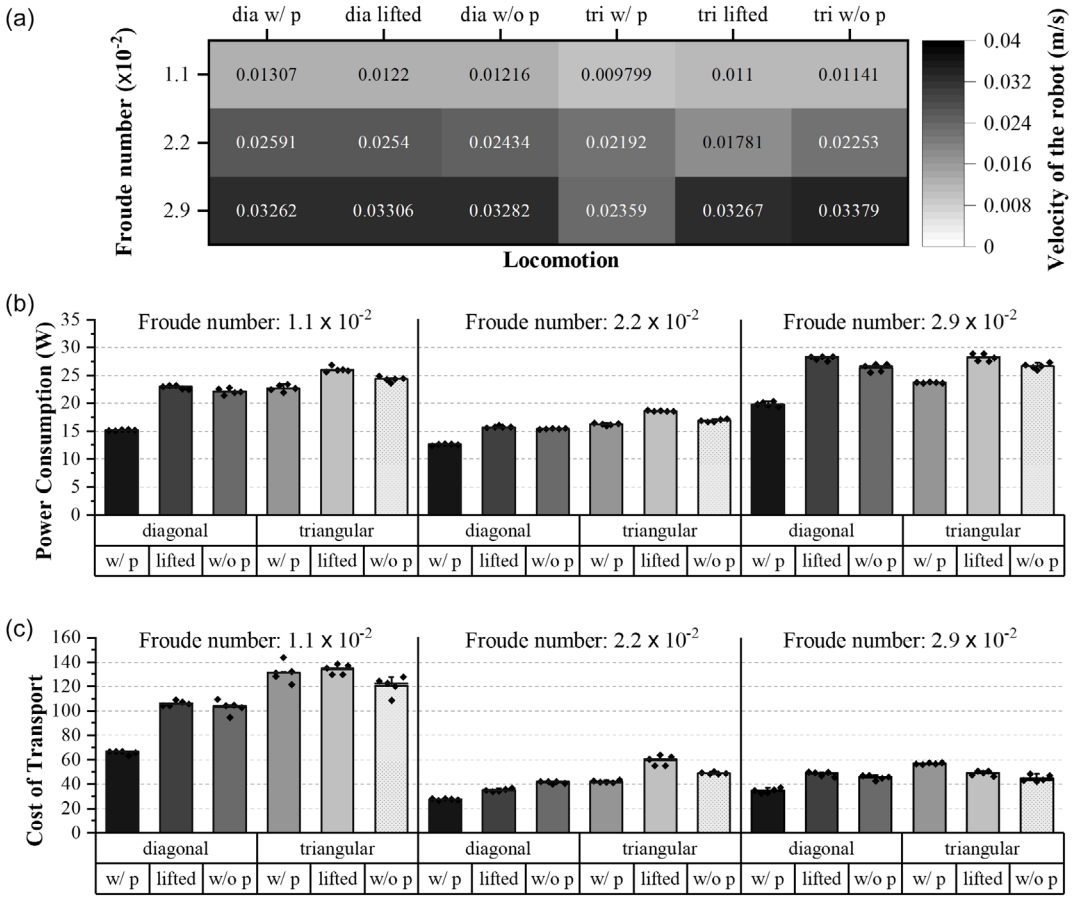


**Figure 6.** Results of the locomotion experiment with varying Froude numbers. a) The average velocities of the robot. b) Power consumption of the robot according to the gait and posture with different Froude numbers. c) The robot's transport cost according to the gait and posture with different Froude numbers.

the diagonal gait consistently showed a lower CoT than the triangular gait when the postures were identical.

Overall, "diagonal w/ p" demonstrated the lowest CoT across varying Froude number conditions. Numerically, in the three Froude number conditions (listed in increasing order), "diagonal w/ p" exhibited CoT reductions of 50.968%, 53.650%, and 29.435% compared to "triangular lifted" locomotion. Specifically, at a Froude number of $2.9 \times 10^{-2}$, where "tri w/ p" had the highest CoT, "diagonal w/ p" showed a 39.283% lower CoT.

## 5. Discussion

### 5.1. Discussion

As described in Section 2.3, the locomotion that affects the robot's CoT is a combination of posture and gait. In this section, based on the results of dynamic simulations and real-world locomotion experiments, we analyze the causes of CoT changes due to postures (including the presence or absence of belly dragging) and gaits. The posture analysis is based on the GRF and torque in the simulation and the power consumption in real-world experiments. For the analysis of the gaits, the joint angular velocities and the robot's locomotion velocity are used. Finally, findings from both analyses are consolidated to discuss why the "dia w/ p" locomotion, which simulates the locomotion of a real tortoise, exhibits the lowest CoT.

#### 5.1.1. Discussion on Posture

In this study's dynamics simulations and locomotion experiments, the "w/ p" posture, which performs belly dragging, consistently showed a lower CoT than those of other postures. An intuitive hypothesis for this phenomenon is the load distribution effect caused by belly dragging. To validate this hypothesis, the GRF and torque were examined in the dynamic simulations.

**Figure 7**a,b shows heatmaps showing the sum of the *z*-axis Euclidean norm of the GRF applied on the four feet and the belly, respectively. Even when the same gait is used, the sum of the Euclidean norm of the GRF applied on the four feet varies depending on whether belly dragging is present. As shown in Figure 7a, the belly-dragging locomotion had smaller GRF than those of other postures with the same gait. In the case of the body length of 0.5 m, the "w/ p" posture showed 56.85% and 51.72% smaller values of GRF compared to the "w/o p" posture in diagonal and triangular gaits, respectively.

As shown in Equation (1), the GRF can directly influence the torque on the joint; thus, these differences in GRF lead to differences in torque. As shown in Figure 7c, when using the same gait, the torques in the "w/ p" posture were the smallest among the three postures. For example, the "w/ p" posture showed 14.88% and 21.85% lower torque sums in diagonal and triangular gaits, respectively, compared to the "w/o p" posture. Similarly, compared to the "lifted" posture, the "w/ p" posture showed 40.26% and 17.66% lower torque sums in diagonal and

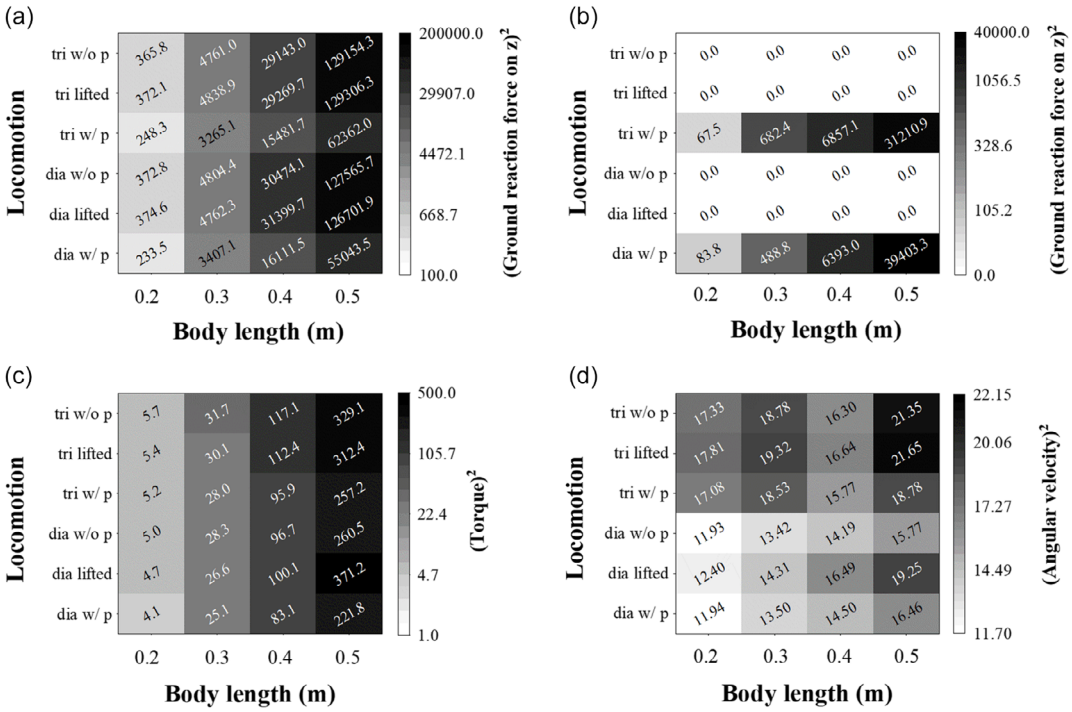


**Figure 7.** Additional results of simulation I (body length simulation) and simulation model performance based on body height offset. a) Heat map of GRF acting on four feet. b) Heat map of GRF acting on belly. c) Heat map of torque acting on joints. d) Heat map of angular velocity. The body masses of the simulation models were 1.1, 3.7, 8.8, and 17.2 kg as the body length increased from 0.2 to 0.5 m, respectively.

triangular gaits, respectively. In summary, the belly-dragging posture distributes the GRF applied on the robot's feet to the belly contact point, thereby reducing the torque applied to the joints of the robot system. The torque applied to the joint is directly proportional to the energy-related numerator of CoT, according to Equation (11). Consequently, it can be determined that the belly-dragging posture reduces CoT from an energy perspective. However, as shown in Figure 3f, when the friction coefficient of the belly increases, friction can cause an increase in the robot's CoT. Therefore, it is important to design a plastron with a low friction coefficient.

The locomotion experiments with the tortoise-inspired robot, conducted under conditions of varying payloads and Froude numbers, showed results similar to the simulations. The "w/ p" posture, which includes belly dragging, consistently exhibited lower power consumption compared to other postures. This suggests that belly dragging reduced power consumption regardless of gait type, environmental conditions, payload, or Froude number. According to Equation (14), consumed power is directly proportional to the numerator of the CoT. Therefore, similar to the simulations, it can be determined that the belly-dragging posture generally reduces CoT from a power perspective. Note that, as mentioned in Section 4.3, there are cases where the "w/ p" posture might increase CoT due to unexpected locomotion hindrances caused by belly dragging. In summary, both simulations and experiments demonstrate that belly dragging in the "w/ p" posture leads to reduced energy and power consumption, highlighting its effectiveness in energy-efficient locomotion.

#### 5.1.2. Discussion on Gait

As shown in Figure 3, 5, and 6, both dynamic simulations and real-world locomotion experiments consistently showed that diagonal gait exhibited lower CoT than that of the triangular gait. This phenomenon was determined to have two main causes. The first cause is related to the differences in joint angular velocities, resulting from the distinct gait cycle characteristics of the two gaits. As shown in Figure 2a,b, during one gait cycle, the triangular gait divides leg movements into four phases, one leg moving at a time, while the diagonal gait divides legs into pairs and moves them in two phases. Therefore, under the same stride frequency conditions, when comparing the swing time of one leg, the triangular gait results in shorter swing times compared to those of the diagonal gait. Furthermore, according to Equation (8), even if the diagonal and triangular gaits have the same stride length, they have different duty factors, leading to leg strokes of 0.65 times and 0.825 times the stride length, respectively. In summary, a leg-performing swing motion in the triangular gait needs to cover a longer distance in a shorter time, resulting in higher joint angular velocities compared to those of the diagonal gait.

This phenomenon can be observed in Figure 7d. Figure 7d presents a heatmap of the sum of squared angular velocities of the joint in Simulation I. When the posture conditions are the same, triangular gait showed higher angular velocities compared to diagonal gait, regardless of the robot's length. According to Equation (11), angular velocities are directly proportional to the energy-related numerator of the CoT. Therefore, higher joint angular velocities in the triangular gait can be considered one of the reasons why the triangular gait results in a higher CoT compared to the diagonal gait.

The second cause is the robot's locomotion velocity, which is influenced by the gait. As shown in Figure 5a and 6a, under the same experimental conditions and posture, the diagonal gait generally demonstrates a higher locomotion velocity than that of the triangular gait. Despite having the same stride length, the difference in the velocity between the two gaits can be attributed to unwanted displacement caused by foot tip slip and belly dragging. The triangular gait has higher joint angular velocities, resulting in relatively faster foot tip velocities. Additionally, due to CoB compensation, the triangular gait involves side-to-side motion, resulting in both forward and vertical movements, which contribute to additional inertia. The faster movement of the foot tip and the additional inertia caused by the triangular gait can result in unwanted displacement of the foot tip. Also, the side-to-side motion caused by CoB compensation during belly-dragging locomotion creates additional friction in the vertical direction, which can reduce the locomotion velocity. For these reasons, the triangular gait tends to have a lower locomotion velocity than that of the diagonal gait. According to Equation (14), locomotion velocity is inversely proportional to CoT. Therefore, the gait-induced locomotion velocity is one of the reasons why the triangular gait tends to have a higher CoT than that of the diagonal gait.

In summary, belly dragging reduces CoT by reducing the GRF applied on the foot tip, the joint torques, and the power consumption. The diagonal gait achieves a lower CoT than that of the triangular gait due to its lower joint angular velocities and faster locomotion velocity. A lower CoT indicates higher locomotion energy efficiency. Therefore, among the six locomotion methods in this study, the tortoise-inspired "dia w/ p" locomotion, which combines belly-dragging and diagonal gait, can be considered an energy-efficient locomotion method. This conclusion has been validated through various simulations with different robot lengths, masses, belly friction coefficients, and Froude numbers, as well as in real-world locomotion experiments.

### 5.2. Discussion on Body Height

As mentioned in Section 3.2, belly dragging may help or interfere with robot locomotion, depending on the body height. In this discussion, we aim to analyze the results of dynamic simulations concerning body height and discuss how belly dragging reduced the CoT. **Figure 8** shows a graph showing CoT, torque squared sum, angular velocity squared sum, velocity, squared sum of *z*-axis GRF on foot, and squared sum of z-axis GRF on the belly, from top to bottom. Figure 8a,b shows results for diagonal and triangular gaits. The black square, blue triangle, and red circle symbols represent results for "w/ p," "w/o p," and "lifted" postures. In the "lifted" posture, the offset $G$ was set at 10.6 mm to implement the posture without belly dragging.

Changes in body height may affect the GRF applied to the belly and the foot. In the following subsections, the effects of

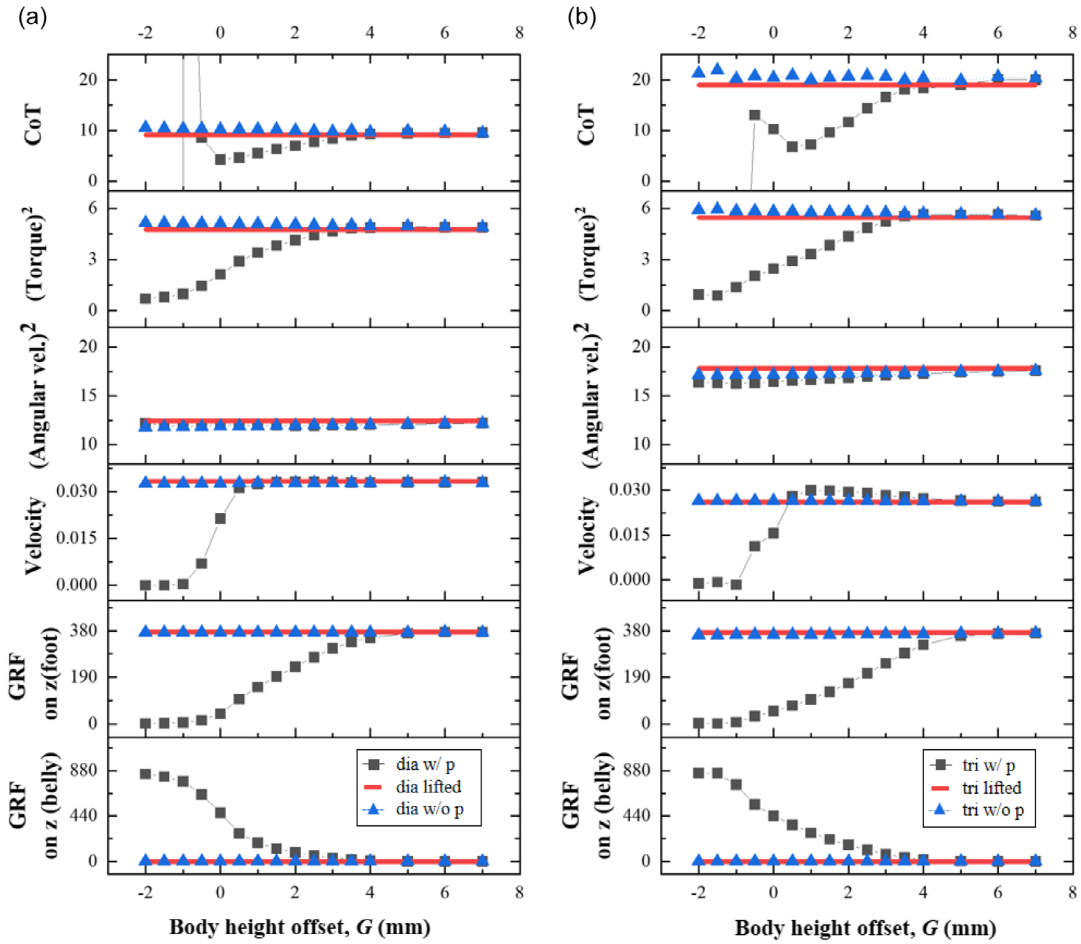


**Figure 8.** Performance of each gait in accordance with body height offset. The body length of the robot, the coefficient of friction on the belly, and the coefficient of friction on the foot were set at 0.2, 0.25, and 1.00 m, respectively. a) Performance of diagonal gait in accordance with body height offset. b) Performance of triangular gait in accordance with body height offset.

body height variation on the CoT were examined based on comparisons between the "w/o p" and "lifted" postures, as well as between the "w/o p" and "w/ p" postures.

### 5.2.1. Postures without Belly Dragging

Since the "w/o p" and "lifted" postures do not involve belly dragging, the effect of body height on CoT, independent of the presence of belly dragging, can be examined by analyzing these two postures. In both gaits in Figure 8, the "w/o p" posture consistently showed higher CoT compared to the "lifted" posture, regardless of the value of $G$. In the case of the diagonal gait, the largest CoT difference between the "w/o p" and "lifted" postures occurred when $G$ was $-2$, with a difference of 14.13%. For the triangular gait, the largest CoT difference occurred when $G$ was $-1.5$, with a difference of 15.05%. The primary reason for these results is the torque difference between the two postures. The torque in the "w/o p" posture was consistently higher than in the "lifted" posture. For the diagonal and triangular gaits, the differences between the sums of the squared torques for "w/o p" and "lifted" were largest at 8.24% and 8.91% when the $G$ values were $-2$ and $-1.5$, respectively.

On the other hand, most of the other metrics, such as angular velocity, GRF on foot, and locomotion velocity, showed relatively small differences between the two postures. The angular velocity and GRF on foot of the "w/o p" posture were consistently smaller than those of the "lifted" posture, with differences of up to 5.11% and 2.59%, respectively, when $G$ was $-2$. Regarding locomotion velocity, in the diagonal gait, the "lifted" posture was faster than the "w/o p" posture, whereas in the triangular gait, the "w/o p" posture was slightly faster than the "lifted" posture. Specifically, when $G$ was $-2$, in the diagonal gait, the "w/o p" posture exhibited a 2.03% slower locomotion velocity than that of the lifted posture while, in the triangular gait, the w/o p posture showed a 1.33% faster locomotion velocity than that of the "lifted" posture.

The "w/o p" and "lifted" postures differ only in the body lift height, meaning the primary variable is the kinematic posture difference. Therefore, it can be inferred that kinematic posture affects the torque applied to the robot joints, which can, in turn, influence the CoT.

#### 5.2.2. Body Height and Belly Dragging

To analyze the effect of belly dragging on CoT based on the body height, the "w/ p" and "w/o p" postures were compared in both gaits. In cases in which $G$ was small ($G \leq 0$), there was a problem of CoT divergence in the "w/ p" posture due to significant disruption of locomotion caused by belly dragging. In contrast, in cases in which $G$ was large ($G \geq 4$), contact between the belly and the ground rarely occurred, resulting in similar outcomes between these two postures. Therefore, selecting $G$ within an appropriate range is crucial for efficient utilization of belly dragging.

When $G$ was selected within the appropriate range ($0 < G < 4$), decreases in foot GRF, torque, and CoT were observed in the "w/ p" posture compared to the "w/o p" posture. For example, in the case of diagonal gait with $G$ of 0.5, the "w/ p" posture showed 72.66%, 43.35%, and 54.78% reductions in GRF on foot, torque, and CoT, respectively, compared to the "w/o p" posture. In contrast, angular velocities and locomotion velocities showed relatively similar values in both postures.

Through the comparison between the "w/o p" and "lifted" postures in Section 5.2.1, it was confirmed that a lower body height increased both CoT and torque, regardless of belly dragging. Furthermore, the comparison between the "w/ p" and "w/o p" postures in Section 5.2.2 revealed that appropriate body height in belly dragging can reduce CoT through the dispersion of GRF to the belly.

However, if the body height is too low and most of the GRF is applied to the belly, this can interfere with locomotion, leading to an increase in CoT. On the other hand, if the body height is too high and there is almost no belly contact, there is little difference between the "w/ p" and "w/o p" postures. Therefore, selecting the optimal body height when performing belly-dragging locomotion is crucial for minimizing CoT and increasing energy efficiency. This could potentially become a new research topic, and future studies may focus on optimizing body height for belly dragging.

## 6. Conclusion

In this study, we aimed to analyze the effect of tortoise locomotion, which is known to be energy efficient, on the energy efficiency of a robot. For this purpose, we designed a tortoise-inspired quadruped robot that can perform belly dragging by simulating the joint structure, plastron, and locomotion of a tortoise. In addition, theory-based dynamic simulations and real-world locomotion experiments were conducted to verify the effect of tortoise locomotion on robot energy efficiency. To ensure the generality of the results, we designed six different locomotion combinations comprising postures and gaits. In the dynamics simulation, we used variables such as the robot body length and mass, friction coefficient of the plastron, and Froude number. We also varied the payload and Froude number of the robot to see if the results were similar to the dynamics analysis in real-world environment.

As a result of the theory-based dynamics simulation, the "dia w/ p" locomotion, which simulates the locomotion of a tortoise, showed the lowest CoT regardless of the length, mass, and Froude number of the robot. In the robot locomotion experiments, the "dia w/ p" locomotion had the lowest CoT in all experimental conditions. This confirms that the locomotion that simulates the belly-dragging and diagonal gait of a real tortoise has higher energy efficiency than other locomotion combinations when applied to a robot.

Since the locomotion designed in this study can be represented by a combination of posture and gait, we analyzed the reasons for this result from the perspective of posture and gait. In the case of belly dragging, represented as "w/ p" among the three postures, we verified that it improves energy efficiency by reducing the GRF applied to the robot's foot tip, torque applied to the joints, and robot power consumption. In this process, we found that the CoT decreased as the friction coefficient of the plastron, responsible for belly dragging, became smaller. We found that diagonal gait has lower joint angular velocity and higher locomotion velocity than triangular gait, resulting in lower CoT.

Thus, both belly dragging, a postural characteristic of tortoises, and their diagonal gait significantly contributed to the robot's lower CoT. Consequently, this implies that the energy-efficient locomotion of tortoises, specifically the diagonal gait coupled with belly dragging, is transferable to robotic platforms to enhance energy efficiency.

This bioinspired robot, with its energy-efficient design inspired by tortoise locomotion, holds great potential in critical applications such as search and rescue operations, space exploration, and payload transportation. In the realm of search and rescue, this robot's capability to endure long operations with minimal energy consumption makes it an invaluable asset. It can navigate through challenging terrains and debris-laden areas with their quadruped gaits, providing essential assistance in disaster-stricken zones while minimizing the risk to human rescuers. In space exploration, this robot's energy efficiency and adaptability to harsh, unfamiliar terrains make it an ideal candidate for exploring the rugged landscapes of other planets, where energy resources are scarce and environmental conditions are extreme. Additionally, in industrial and logistic sectors, the robot's enhanced payload capacity, a direct benefit of its energy-efficient design, offers a sustainable solution for transporting materials and equipment over extended periods and distances. This capability not only streamlines operational efficiency but also aligns with the increasing focus on sustainability and energy conservation in technological advancements. Especially, as demonstrated in this study, the increase in energy efficiency and payload capacity through a locomotion strategy that incorporates both belly-dragging and diagonal gait can be effectively combined with other research that enhances energy efficiency through mechanical structures or control strategies.

## Supporting Information

Supporting Information is available from the Wiley Online Library or from the author.

## Conflict of Interest

The authors declare no conflict of interest.

## Data Availability Statement

Research data are not shared.

## Keywords

biomimetic and bioinspired robotics, designs, mechanisms, mobility and locomotions, modeling and controls

Received: November 2, 2023
Revised: January 16, 2024
Published online: March 8, 2024

[1] N. Mazouchova, P. B. Umbanhowar, D. I. Goldman, *Bioinspir. Biomim.* **2013**, *8*, 026007.
[2] J. A. Nyakatura, K. Melo, T. Horvat, K. Karakasiliotis, V. R. Allen, A. Andikfar, E. Andrada, P. Arnold, J. Lauströer, J. R. Hutchinson, M. S. Fischer, A. J. Ijspeert, *Nature* **2019**, *565*, 351.
[3] Z. Chen, T. Fan, X. Zhao, J. Liang, C. Shen, H. Chen, D. Manocha, J. Pan, W. Zhang, *IEEE Access* **2021**, *9*, 8392.
[4] J. Hooks, M. S. Ahn, J. Yu, X. Zhang, T. Zhu, H. Chae, D. Hong, *IEEE Robot. Autom. Lett.* **2020**, *5*, 5409.
[5] M. Hutter, C. Gehring, A. Lauber, F. Gunther, C. D. Bellicoso, V. Tsounis, P. Fankhauser, R. Diethelm, S. Bachmann, M. Bloesch, L. Isler, K. Meyer, *Adv. Robot.* **2017**, *31*, 918.
[6] D. Owaki, A. Ishiguro, *Sci. Rep.* **2017**, *7*, 1.
[7] Z. Tang, P. Qi, J. Dai, *Indust. Robot.: Int. J.* **2017**, *44*, 512.
[8] K. Xu, H. Ma, J. Chen, W. Zhang, H. Deng, X. Ding, in *2018 Inter. Conf. on Reconfigurable Mechanisms and Robots (ReMAR)*, Delft, Netherlands, June **2018**.
[9] A. N. Sarmah, A. Boruah, D. Kalita, D. Neog, S. Paul, *Procedia Comput. Sci.* **2018**, *143*, 671.
[10] A. Fukuhara, Y. Masuda, M. Gunji, K. Tadakuma, A. Ishiguro, in *2020 IEEE/SICE Inter. Symp. on System Integration (SII)*, IEEE, Piscataway, NJ **2020**.
[11] B. J. Smith, J. R. Usherwood, *Bioinspir. Biomim.* **2020**, *15*, 026004.
[12] X. Bin Peng, E. Coumans, T. Zhang, T.-W. Lee, J. Tan, S. Levine, in *Robot.: Sci. Syst. XVI* , Corvalis, OR, July **2020**.
[13] H. Xing, S. Guo, L. Shi, Y. He, S. Su, Z. Chen, X. Hou, *Appl. Sci.* **2018**, *8*, 156.
[14] H. Xing, S. Guo, L. Shi, X. Hou, Y. Liu, H. Liu, Y. Hu, D. Xia, Z. Li, in *2019 IEEE/RSJ Inter. Conf. on Intelligent Robots and Systems (IROS)*, IEEE, Piscataway, NJ **2019**.
[15] R. Baines, S. K. Patiballa, J. Booth, L. Ramirez, T. Sipple, A. Garcia, F. Fish, R. Kramer-Bottiglio, *Nature* **2022**, *610*, 283.
[16] K. Kiguchi, Y. Kusumoto, K. Watanabe, K. Izumi, T. Fukuda, *Artif. Life Robot.* **2002**, *6*, 120.
[17] S. Kitano, S. Hirose, A. Horigome, G. Endo, *ROBOMECH J.* **2016**, *3*, 1.
[18] N. Kashiri, A. Abate, S. J. Abram, A. Albu-Schaffer, P. J. Clary, M. Daley, S. Faraji, R. Furnemont, M. Garabini, H. Geyer, A. M. Grabowski, J. Hurst, J. Malzahn, G. Mathijssen, D. Remy, W. Roozing, M. Shahbazi, S. N. Simha, J. B. Song, N. Smit-Anseeuw, S. Stramigioli, B. Vanderborght, Y. Yesilevskiy, N. Tsagarakis, *Front. Robot. AI* **2018**, *5*, 129.
[19] D. Yun, R. S. Fearing, in *2015 IEEE Inter. Conf. on Advanced Intelligent Mechatronics (AIM)*, IEEE, Piscataway, NJ **2015**.
[20] C. Hubicki, J. Grimes, M. Jones, D. Renjewski, A. Spröwitz, A. Abate, J. Hurst, *Int. J. Robot. Res.* **2016**, *35*, 1497.
[21] A. Badri-Spröwitz, A. A. Sarvestani, M. Sitti, M. A. Daley, *Sci. Robot.* **2022**, *7*, 64.
[22] G. Gabrielli, T. Von, *What price speed?: Specific power required for propulsion of vehicles*, **1950**.
[23] J. Rubenson, D. B. Heliams, D. G. Lloyd, P. A. Fournier, *Proc.: Biol. Sci.* **2004**, *271*, 1091.
[24] B. Goldberg, R. Zufferey, N. Doshi, E. F. Helbling, G. Whittredge, M. Kovac, R. J. Wood, *IEEE Robot. Autom. Lett.* **2018**, *3*, 987.
[25] R. C. Woledge, N. A. Curtin, E. Homsher, *Energetic Aspects of Muscle Contraction*, Academic Press, Cambridge **1985**.
[26] R. J. Full, *The Concepts of Efficiency and Economy in Land Locomotion*, Cambridge University Press, Cambridge **1992**, pp. 97–132.
[27] R. V. Baudinette, A. M. Miller, M. P. Sarre, *Physiol. Biochem. Zool.* **2000**, *73*, 672.
[28] H. Ewart, P. Tickle, R. Nudds, W. Sellers, D. Crossley, J. Codd, *Biology* **2022**, *11*, 1052.
[29] R. M. Alexander, *Chapter 2. Muscle, The Motor*, Princeton University Press, Princeton, NJ **2003**.
[30] R. C. Woledge, *J. Physiol.* **1968**, *197*, 685.
[31] L. O. Nwoye, G. Goldspink, *Experientia* **1981**, *37*, 856.
[32] R. M. Alexander, *Chapter 1. The Best Way to Travel*, Princeton University Press, Princeton, NJ **2003**.
[33] J. A. Nyakatura, E. Andrada, S. Curth, M. S. Fischer, *Evol. Biol.* **2013**, *41*, 175.
[34] L. Dalla Valle, A. Nardi, M. Toni, D. Emera, L. Alibardi, *J. Anat.* **2009**, *214*, 284.
[35] E. Dickinson, C. S. Hanna, H. M. Fischer, E. C. Davoli, A. A. Currier, M. C. Granatosky, *J. Exp. Zool., Part A: Ecol. Integr. Physiol.* **2022**, *337*, 329.
[36] M. Biaggini, C. Corti, *Herpetol. Conserv. Biol.* **2018**, *13*, 539.
[37] R. M. Alexander, *J. Robot. Soc. Jpn* **1993**, *11*, 314.
[38] A. S. Jayes, R. M. Alexander, *J. Zool.* **1980**, *191*, 353.
[39] W. O. Walker, *Ohio J. Sci.* **1972**, *72*, 177.
[40] R. M. Alexander, A. Jayes, *J. Biomech.* **1980**, *13*, 383.
[41] R. M. Alexander, *Int. J. Robot. Res.* **1984**, *3*, 49.
[42] T. M. Inc., Matlab version: 9.11.0 (r2021b), **2021**, https://www.mathworks.com.
[43] R. Featherstone, Spatial v2 (version 2), **2012**.
[44] R. Featherstone, *Rigid Body Dynamics Algorithms*, Springer, Berlin **2014**.
[45] M. Azad, R. Featherstone, *IEEE Trans. Robot.* **2013**, *30*, 736.
[46] V. Vasilopoulos, I. S. Paraskevas, E. G. Papadopoulos, *Robot. Auton. Syst.* **2018**, *102*, 13.
[47] M. Azad, M. N. Mistry, in *2015 IEEE Inter. Conf. on Robotics and Automation (ICRA)*, IEEE, Piscataway, NJ **2015**, pp. 4391–4396.
[48] R. M. Alexander, *Chapter 4. Consequences of Size Differences*, Princeton University Press, Princeton, NJ **2003**.
[49] J. Ramos, S. Kim, *IEEE Robot. Autom. Lett.* **2018**, *3*, 3293.
[50] K. J. Waldron, C. Hubert, in *Proc. 2000 ICRA. Millennium Conf. IEEE Inter. Conf. on Robotics and Automation. Symposia Proceedings (Cat. No. 00CH37065)*, IEEE, Piscataway, NJ **2000**, Vol. *1*, pp. 40–45.
[51] M. Haberland, S. Kim, *Bioinspir. Biomim.* **2015**, *10*, 016011.
[52] K. Wren, D. L. Claussen, M. Kurz, *J. Herpetol.* **1998**, *32*, 144.
[53] P. G. De Santos, E. Garcia, J. Estremera, *Quadrupedal Locomotion: An Introduction to the Control of Four-Legged Robots*, Vol. *1*, Springer, Berlin **2006**.